Ketoprofen poly(lactide-co-glycolide) physical interaction studied by Brillouin spectroscopy and molecular dynamics simulations

Paolo Blasi[a,1], Serena Casagrande[b,2], Alessandro Pedretti[c], Daniele Fioretto[d], Giulio Vistoli[c], Silvia Corezzi[d*]

[a] Scuola del Farmaco e dei Prodotti della Salute; Università degli Studi di Camerino, 62032 - Camerino, Italy.

[1] Present address: Dipartimento di Farmacia e Biotecnologie, Alma Mater Studiorum - Università di Bologna, 40127 - Bologna, Italy.

[b] Dipartimento di Scienze Farmaceutiche, Università degli Studi di Perugia, 06123 - Perugia, Italy.

[2] Present address: Pizeta Pharma S.p.A., Ponte San Giovanni, 06135 - Perugia, Italy.

[c] Dipartimento di Scienze Farmaceutiche "Pietro Pratesi", Università degli Studi di Milano, 20133 - Milano, Italy.

[d] Dipartimento di Fisica e Geologia, Università degli Studi di Perugia, 06123 - Perugia, Italy.

*Author to whom correspondence should be addressed:

Silvia Corezzi, e-mail: silvia.corezzi@unipg.it, phone: +390755852799

ABSTRACT

The performances of poly(lactic-co-glycolic acid) drug delivery systems are affected by the molecular interactions established between the drug and the polymer matrix as well as by the physical state of the drug embedded. Indeed, the drug may induce polymer plasticization with a drastic change in the release kinetics and medicinal product performances. The aim of this study was to better understand the interactions between poly(lactic-co-glycolic acid) and ketoprofen, the latter known to plasticize hydrophilic and hydrophobic polymers. Ketoprofen interacts with poly(lactic-co-glycolic acid) exerting a maximum plasticizing effect at weight fractions around 0.25. Higher ketoprofen amounts form heterogeneous mixtures with the non-soluble molecules dispersed in the matrix as crystals or amorphous domains, depending on the preparation method. Unexpectedly, the amorphous ketoprofen dispersed in the poly(lactic-co-glycolic acid) matrix was remarkably stable. H-bonding seems responsible for the glass transition temperature reduction and the limited solubility. Brillouin spectroscopy and molecular dynamics simulation data suggest that ketoprofen solubility increases with temperature and non-polar interactions are responsible for this phenomenon.

Keywords:

poly(lactic-co-glycolic acid), PLGA, glass transition, amorphous stability, Brillouin light scattering, molecular dynamics.

1. **INTRODUCTION**

Polymers have been employed in the production of medicinal products for centuries and, among the excipients used in formulation, they are essential materials. Even advanced formulations, known as drug delivery systems (DDSs), take advantage of the peculiar characteristics of macromolecules to modulate site, time and/or rate of drug release in the body (Debotton and Dahan, 2017; Liechty et al., 2010). Despite the large use of amorphous and semi-crystalline polymers in formulation and drug delivery, a complete understanding of their behaviour when they come in intimate contact with other excipients or active pharmaceutical ingredients (APIs) is still missing. This is in part due to an incomplete understanding of the physics behind the glass transition (Ngai, 2007a, 2007b), a fundamental phenomenon to deal with when using amorphous and semi-crystalline polymers.

The interaction between polymeric excipients and APIs may lead to degradation (e.g., hydrolysis, oxidation), crystallization and isomerization of the latter, compromising the efficacy and potential toxicity of the medicinal product (Crowley and Martini, 2001). On the other hand, these interactions may change the polymer's chemical, physical and mechanical behaviour with profound modifications of the formulation or delivery system performances.

Due to a great interest in formulating low water-soluble APIs in amorphous polymers (solid dispersions or solid solutions), to increase API's dissolution rate and apparent solubility, a large body of literature on API/hydrophilic polymer interactions is now available (Hancock and Zografi, 1991; Qian et al., 2010; Knopp et al., 2015; Kawakami, 2019). From the polymer point of view, these interactions might have an effect on the glass transition temperature (T_g) leading to its decrease (plasticizing effect) (Wu and McGinity, 1999) or increase (antiplasticizing effect) (Ueda et al., 2014).

To obtain API long-term and controlled release, many DDSs take advantage of hydrophobic polymers, such as poly(lactic-co-glycolic acid) (PLGA), polycaprolactone, and polyhydroxybutarate valerate (Kamaly et al., 2016). However, in the case of hydrophobic macromolecules, polymer-drug interactions have received less attention by the research community and a lack of knowledge is

perceptible. We believe that this gap cannot be filled by simply translating the information gained on hydrophilic polymers to hydrophobic ones.

PLGA is a hydrophobic biodegradable polymer intensively studied in the last 50 years and largely used in the manufacturing of microparticles and other kinds of DDSs already employed in the clinical practice (Blasi, 2019). Different cases of polymer/drug interaction with detrimental effects on the performance of the manufactured system have been described (Fernández-Carballido et al., 2004; Selmin et al., 2012; Siegel et al., 2016). From the macromolecule point of view, such interactions may change the physico-chemical and/or the mechanical features of the polymer, with negative outcome on the device performances (Alexis, 2005). For instance, a shift in T_g may have serious consequences in the polymer degradation rate and in the rate and mechanisms of drug release (Ricci et al., 2005; Gasmi et al., 2015). A change of the polymer chains dynamics may also alter the physical state of the embedded drug (from crystalline to amorphous) or the polymer/drug solubility with additional negative consequences for the control of the release (Gasmi et al., 2015).

The aim of this study was to better understand the interactions between PLGA and ketoprofen (KET), a non-steroidal anti-inflammatory drug known to have a plasticizing effect on both hydrophilic and hydrophobic polymers (Blasi et al., 2007; Gue et al., 2013, 2015; Gasmi et al., 2015). To this end, here we report the results of the characterization of PLGA/KET **(Figure S1)** binary mixtures performed by common techniques employed to study drug-polymer systems (i.e., calorimetry and microscopy) and by means of temperature-scanning Brillouin light scattering (BLS) spectroscopy, a hitherto neglected technique that can provide interesting physico-chemical and molecular insights. Besides, to shed light on the nature of PLGA/KET molecular interactions, molecular dynamics (MD) simulations in which PLGA oligomers were solvated with KET molecules, were performed.

2. MATERIALS AND METHODS

2.1. Experiments

2.1.1. Materials

Poly(D,L-lactide-co-glycolide) (PLGA) 50:50 Resomer® RG 504 (M_w 40-50 kDa; ester terminated), poly(D,L-lactide) Resomer® R 202 H (M_w 10-18 kDa; acid terminated) and poly(D,L-lactide) Resomer® R 202 S (M_w 10-18 kDa; ester terminated) were supplied by Boehringer Ingelheim (Ingelheim, Germany). Prior to use, the polymer was dried under vacuum for 24 h to eliminate traces of moisture. Ketoprofen (KET) was kindly provided by Bidachem SpA (Bergamo, Italy), while methylene chloride (CH_2Cl_2) was supplied by Sigma-Aldrich (Milan, Italy).

2.1.2. Film preparation

PLGA films containing different amounts of KET were casted on silica slides using the solvent casting technique: desired amounts of PLGA and KET (total mass of 0,1 g) were dissolved in 1 mL of CH_2Cl_2 to obtain a highly viscous solution. The solution was deposited on the support and CH_2Cl_2 was allowed to evaporate over-night at room temperature and 24 h under vacuum to remove any residual trace of solvent (Blasi et al., 2007). KET was added at 5, 10, 15, 25, 35 and 50 % (w/w). Pure KET and pure PLGA were processed as described above.

2.1.3. Calorimetry

Thermal behaviour of PLGA/KET films was investigated by differential scanning calorimetry (DSC) using a Mettler 821e (Mettler-Toledo, Greifensee, Switzerland) calorimeter equipped with a liquid nitrogen cooling system. The CH_2Cl_2 polymer solutions (about 5 mg of solid material) containing the desired amounts of KET were directly casted in aluminium pans and treated as described above. After CH_2Cl_2 evaporation, pans were closed with holed lids. An empty sealed aluminium pan was used as a reference. To erase the polymer thermo-mechanical history, samples were subjected to a first

heating ramp, from 25 to 120 °C at 10 °C/min. After an isotherm at 120 °C of 30 min, samples were cooled from 120 to -100 °C and heated again to 120 °C at 10 °C/min. KET melting temperature (T_m) and enthalpy of fusion (ΔH_m) were determined on the first heating ramp, while T_g values of PLGA, KET and PLGA/KET mixtures were determined on the second heating ramp as the midpoint of the baseline shift. After measurements, films were stored in a hermetic chamber in absence of humidity (P_2O_5) at room temperature and characterized again by DSC using heating and cooling cycles as described above. Data were elaborated with STAR^e software (Mettler Toledo, Griefensee, Switzerland), and the results were the mean ± SE of three independent measurements.

2.1.4. 3D-scanning electron microscopy

Film surface morphology was investigated by a field emission scanning electron microscope (FESEM) LEO 1525 equipped with a GEMINI column (ZEISS, Germany) equipped with an AsB®/4QBS detector with 3D Surface Modelling software (ver. 1.5.4). Samples were prepared by casting the polymer, KET, and polymer/KET solutions on a glass slide attached to an aluminium specimen stub by a double sided adhesive carbon disc. CH_2Cl_2 was allowed to evaporate over-night at room temperature and 24 h under vacuum to remove any residual trace of solvent. Films were sputter coated with gold prior to imaging (Emitech K-550X sputter coater; Emitech, Ashford, UK). Coating was performed at 20 mA for 4 minutes.

2.1.5. Brillouin light scattering spectroscopy

Acoustic properties of PLGA, KET and PLGA/KET samples were investigated by means of Brillouin light scattering (BLS). A single mode laser operating at λ_i=532 nm was used, and the light scattered from the sample in a backscattering geometry was analysed by a Sandercock type (3+3)pass tandem Fabry-Perot interferometer, characterized by a finesse of ~100 and a contrast ratio greater than 10^{10} (Castiglia et al., 2001). Each sample was heated at 120 °C, left at this temperature for 30 min, and then cooled down to below -60 °C at a rate of 1 °C/min.

The acquisition of BLS spectra (duration of each acquisition 30 s, to ensure a good signal-to-noise ratio) was performed at regular temperature intervals. The technique reveals light inelastically scattered by refractive index fluctuations produced by thermally activated acoustic waves. In the ideal case of undamped acoustic modes, i.e. when the sound waves propagate in the material in the absence of attenuation mechanisms, from energy and momentum conservation laws very sharp maxima (Brillouin peaks) in the intensity of backscattered light are expected at frequencies shifted with respect to the incident light by a quantity f given by $\omega_0 = 2\pi f = \pm v_L q$, where v_L is the velocity of the longitudinal acoustic wave, $q=4\pi n/\lambda_i$ is the phonon-photon exchanged wavevector, and n is the refractive index of the sample. In the more realistic case in which light is scattered by attenuated acoustic modes, a peak broadening is observed. In this case the Brillouin frequency f, related to the apparent longitudinal sound velocity v_L, and the peak width, related to the sound wave attenuation, are derived by fitting the spectrum $I(\omega)$ by a damped harmonic oscillator lineshape (with undamped frequency ω_0) convoluted with the response function $R(\omega)$ of the interferometer (Fioretto et al., 1999):

$$I(\omega) = \frac{I_0}{\pi} \frac{\omega_0^2 \Gamma}{(\omega^2 - \omega_0^2)^2 + \omega^2 \Gamma^2} \otimes R(\omega) \qquad \textbf{Eq. 1}$$

Here, I_0 is an intensity factor dependent on the scattering cross-section, while ω_0 and Γ approximately give the position and full-width-at-half-maximum (FWHM) of the peaks.

In transparent samples, Eq.1 properly describes the whole BLS spectrum in the high temperature, relaxed regime, and also provides a good approximation of the spectrum around the maximum of the Brillouin peaks in the presence of relaxation processes. In the last case, the parameters ω_0 and Γ can be used to calculate the real and imaginary part of the longitudinal modulus at the frequency of the Brillouin peak, through the relations (Fioretto et al., 1999):

$$M'(\omega_0) = \rho\omega_0^2/q^2 \quad ; \quad M''(\omega_0) = \rho\omega_0\Gamma/q^2 \qquad \textbf{Eq. 2}$$

where ρ is the mass density.

It is worth noticing that two characteristic length scales are relevant in our BLS experiment. The first is the wavelength of the acoustic modes probed by BLS (≈200 nm, comparable with that of the laser light), involving the collective motion of molecules that propagates in the sample through a distance of at least a few wavelengths. Heterogeneities of this size in the sample can be responsible for multiple scattering processes and nonlinear sound dispersion phenomena. The second characteristic length scale is given by the scattering volume, which is a few hundred microns in our experiment, due to the optics adopted. Therefore, sample heterogeneities with size between a few microns and hundred microns give rise to different peaks in the spectrum, one for each homogeneous region within the scattering volume.

2.2. Numerical simulations

2.2.1. PLGA system: initial construction

A 16-mer starting sequence was manually generated, respecting the 50:50 molar composition of Resomer® RG 504. The stereochemical configuration was assigned so as to lead to an atactic copolymer with isotactic dyad probabilities of 50%. The single oligomer was then minimized in its refined helical geometry as recently reported (Lange et al., 2016). Such a conformation should allow an optimal inter-helical complementarity in the formation of the six oligomers bundle. The bundle was generated by progressive docking simulations as performed by PLANTS using the ChemPLP score function and generating 10 complexes in each calculation (Korb et al., 2009). The so-obtained best bundle was finally minimized and inserted into a 70 Å side box containing 1880 CCl_4 molecules, using the VEGA suite of programs (Pedretti et al., 2002). The systems were minimized to optimize the relative position of the solvent molecules and underwent 30 ns MD runs at the four different temperatures, namely 295, 335, 375 and 415 K. The MD simulations had the general characteristics as described below. The last frame of each MD run was finally minimized and, after removing the CCl_4 molecules, utilized in the generation of the PLGA/KET systems.

2.2.2. PLGA/KET systems: construction and MD simulations

KET was built in its neutral form and optimized by PM7-based semi-empirical calculations which were also exploited to generate the corresponding dimer (Stewart, 2013). The optimized dimer was then used to build the solvent box by multiplying 10 times the dimer unit on the 3 axes, thus obtaining a 105 Å side cubic system composed of 2000 KET molecules. The KET configuration was assigned randomly by using a purposely developed VEGA script so as the box comprised a perfectly racemic mixture. The so generated box was then minimized and underwent a 50 ns MD simulation to optimize the relative position of KET molecules. The last frame was minimized and utilized to solvate the PLGA bundles obtained by the previous MD runs at the four temperatures investigated by generating 75 Å side cubic boxes in which the PLGA bundles were surrounded by about 850 KET molecules. The obtained PLGA/KET systems were minimized and underwent 50 ns MD runs at the four considered temperatures, namely 295, 335, 375 and 415 K.

All mentioned MD simulations had the following characteristics: (a) periodic boundary conditions (80 Å x 80 Å x 80 Å for PLGA/CCl_4 and PLGA/KET systems and 110 Å x 110 Å x 110 Å for the KET box) were introduced to stabilize the simulation space; (b) Newton's equation was integrated using the r-RESPA method (every 4 fs for long-range electrostatic forces, 2 fs for short-range non bonded forces, and 1 fs for bonded forces); (c) the long-range electrostatic potential was treated by the Particle Mesh Ewald summation method (80 Å x 80 Å x 80 Å for PLGA/CCl_4 and PLGA/KET systems and 110 Å x 110 Å x 110 Å for the KET box); (d) the selected temperatures were maintained within ± 10 K by means of the Langevin's algorithm; (e) Lennard-Jones (L-J) interactions were calculated with a cut-off of 10 Å and the pair list was updated every 20 iterations; (f) a frame was stored every 10 ps thus generating 3000 or 5000 frames; and (g) no constraints were applied to the systems.

The simulations were carried out in two phases: an initial period of heating in which the defined temperatures were reached by increasing 1 K per ps, and the monitored phase of 30 or 50 ns. The

mentioned minimizations were performed using the conjugate gradient algorithm until the r.m.s. gradient was smaller than 0.01 kcal $mol^{-1}Å^{-1}$. All calculations were carried out by NAMD 2.11 with the force-field CHARMM (v. 22) and the Gasteiger's atomic charges (Gasteiger and Marsili, 1978; Phillips et al., 2005). Finally, the calculation of the radial pair distributions was performed by using VMD, while the surface analysis of the MD trajectories was performed by using the VEGA suite of programs.

3. RESULTS AND DISCUSSION

3.1. DSC and microscopy

When KET was mixed with PLGA, a reduction of the polymer T_g was observed (**Figure 1**). A reduction in the T_g value was already evident in the film containing 5% (w/w) of KET (ΔT_g ~ 6 °C) and, with increasing the KET amount, the value progressively decreased reaching a maximum T_g reduction at a KET content around 25% (w/w) **(Table S1)** (Blasi et al., 2007; Gasmi et al., 2015). In mixtures containing KET amounts lower than 25% (w/w), DSC data showed a single T_g, (also known as $T_{g\text{-}mix}$) due to the formation of a homogeneous PLGA/KET system **(Figure 1)**. This indicates that KET is molecularly dispersed in the matrix and interacts with the polymer chains acting as a plasticizer (Blasi et al., 2007). At higher KET percentages, $T_{g\text{-}mix}$ became constant, showing only non-significant fluctuations, and suggesting the overcoming of the solubility limit and the formation of a biphasic system, consisting of amorphous KET domains dispersed in a
PLGA/KET homogeneous mixture. In fact, two distinct thermal transitions, one ascribable to PLGA/KET $T_{g\text{-}mix}$ and another associated to KET T_g were clearly detected **(Figure 1)**.

To have information on the KET physical state after film casting (before thermal treatment), data from the first heating ramp were also analysed. PLGA/KET systems containing higher than 25% (w/w) of KET showed an endothermic event ascribable to KET melting **(Table S1)**, meaning that, during solvent casting, the amount of KET exceeding the solubility limit was able to crystallize within the matrix. In fact, films of pure PLGA or with KET content in the range 5-25% (w/w) presented a smooth surface, while at higher percentages (KET ≥ 35% w/w) KET crystallization could be hypothesized from the high roughness of the film surface **(Figure 2)**.

During solvent casting, CH_2Cl_2 evaporation provoked an increase in concentration of PLGA and KET that start to precipitate when their solubility limits are exceeded. Since CH_2Cl_2 is a good solvent for both components, it is expected to be an excellent plasticizer. CH_2Cl_2 plasticization during film formation induces a high molecular mobility that allows the rearrangement of noninteracting KET

molecules into dimers, essential for unit cell formation (Briard and Rossi, 1990), and the crystal growth in constrained conditions. When the films were heated to a temperature higher than KET T_m (~ 95 °C) and left to stabilize for 30 min at 120 °C to erase their thermomechanical history, the heterogenous system originally formed by solvent evaporation (KET crystals in PLGA/KET matrix) was transformed in a mixture of two amorphous phases: amorphous
KET in PLGA/KET matrix. The existence of amorphous KET was confirmed by the presence of the KET T_g and the absence of KET melting endothermic events in the DSC data of the second heating ramp **(Table S1)**.

So, the preparation method has a critical role in determining the chemical, physical and mechanical properties of the polymer/drug system produced. From the pharmaceutical point of view, it is extremely interesting to highlight that both pure amorphous KET and amorphous KET domains within the PLGA/KET matrix did not crystallize and remained stable at room temperature for at least 2 months **(Table S2)**. This behaviour can be of limited interest in the field of PLGA microparticles, where most of the preparation methods employ the evaporation of a solvent as a crucial step for microparticle formation (Schoubben et al., 2019), but is surely important when the polymer and the API are melted together during manufacturing such as in hot-melt extrusion or in 3D printing technologies (Gue et al., 2013; Guo et al., 2017; Lim et al., 2018).

Interestingly, films loaded with 35 and 50 % (w/w) of KET showed a temperature dependent heterogeneity visible to the eye. Below ~70 °C, the films were opaque while at higher temperatures they became transparent. This phenomenon was reversible. Such a macroscopic characteristic is generally attributed to the formation of micro-heterogeneous (Papkov et al., 1998) or homogeneous monophasic systems (Wahab et al., 2003). This suggests two possible scenarios: i) upon heating the higher mobility of the PLGA/KET matrix allows amorphous KET to disperse in very tiny domains (increased miscibility) and ii) upon heating the higher mobility of the PLGA/KET matrix allows a higher amount (> 25 % w/w) of KET to disperse molecularly (increased solubility). The latter

hypothesis, i.e., the increase of KET solubility in the plasticized PLGA matrix with the rise of temperature, is certainly most reasonable.

The molecular features responsible for PLGA/KET interactions determine both the KET solubility in the matrix and the KET plasticizing effect. The KET ability to act as a plasticizer seems, at least in part, linked to its arylpropionic structure. Indeed, other compounds with the same pharmacophore (arylpropionic acid) display similar plasticizing properties (Kunze et al., 2002; Wu and McGinity, 2001). The carboxylic and ketonic molecular moieties seem to have a role in conferring the plasticizing characteristics to certain molecules, including KET (Tarvainem et al., 2001; Di Martino et al., 2004; Blasi et al., 2007).

3.2 Brillouin spectroscopy

An example of BLS spectra during a temperature scan from 120 to -60 °C is reported in **Figure 3**. The system showed a typical viscoelastic behaviour, with a marked increase of the BLS frequency (from about 10 to 16 GHz) and a reduction of the peak linewidth (from ~3 to <1 GHz) when passing from the fluid to the glassy phase across T_g.

Upon cooling from 120 °C, the pure constituents (i.e., PLGA and KET) and all the PLGA/KET mixtures did not show any signature of crystallization, strengthening the results obtained by calorimetry. At high temperatures, it was noted the presence of the Mountain mode centred at zero frequency, whose linewidth is proportional to the characteristic rate of the structural α-relaxation. Approaching T_g, this rate progressively decreased, and the Mountain mode was squeezed inside the central part of the spectrum, and eventually masked by the intense quasielastic peak (for clarity, not shown in **Figure 3**). The glass transition occurs when this rate decreases below fractions of Hz, and the system can no longer equilibrate upon further cooling.

All samples were transparent above the KET T_m (95 °C) but only those containing KET percentages up to 25% (w/w) remained transparent in the whole scanned temperature range. At higher KET concentrations, there was a temperature below which the components were only partially soluble. As previously stated, opacity is a macroscopic evidence of phase separation with the formation of heterogeneities with size of the order of, or greater than, 1 μm. Such heterogeneity, which develops in samples with KET content > 25% (w/w), produced disordered effects of light scattering and gave rise to broadening of the BLS spectra due to light contributions that underwent multiple scattering inside the sample. As an example, **Figure 4A** shows the comparison between spectra of PLGA with 25 and 50% of KET at high temperature, where both samples had a homogeneous structure, and at low temperature, where one sample was homogeneous and the other non-homogeneous. To quantify this broadening effect, the FWHM of the peaks was compared with the parameter Γ (Eq.1) obtained by fitting only the peaks' higher frequency part and leaving out contributions coming from light scattered at θ < 180° (Corezzi et al., 2018). **Figure 4B** shows that the FWHM in samples at 35 and 50% of KET is in good agreement with the value of Γ at high temperatures, but it receives a significant extra contribution when cooling below 57 °C and 92 °C, respectively. These temperatures well correspond to the onset of opacity in the samples. Noteworthy, the phase separation (i.e., demixing) clearly detected by the temperature-scanning BLS technique, did not correspond to an evident signature in the DSC data (Gasmi et al., 2015). Indeed, to determine or predict API-polymer solubility by calorimetry, proper experimental methodologies (e.g., recrystallization method and dissolution end point method) have been developed (Knopp et al., 2015).

By using Eq.1, the BLS frequency *f* as a function of temperature was obtained for all PLGA/KET mixtures **(Figure 5A)**. In the case of spectra affected by multiple scattering, as noted above, the fit was limited to the high frequency side of the Brillouin peaks, the only part that conveys information from back-scattering processes. The T_g is clearly signalled by a bend in the behaviour of *f*(T): it is approximately linear both above and below T_g, with a slope much less negative in the glassy than in

the rubbery state. For samples with KET content up to 25% (w/w) a change in the slope occurs at a temperature very close to the T_g value measured by DSC, while in biphasic mixtures containing higher KET amounts, the change occurs over a wider temperature interval and there is no a clear evidence of two changes in the slope. More information could be obtained from a derivative analysis showing very similar rates of BLS frequency variation, -d*f*/dT, in all mixtures, with a neat jump that moved to lower temperatures by increasing the KET content **(Figure 5B)**. The shape of the curves for samples with KET < 25% (w/w) showed no appreciable difference and a temperature shift generated a master curve **(Figure 5C)**. This indicates that, at these concentrations, KET mainly exerts a plasticizing effect. The midpoint temperature, in agreement with an equal area construction, can be taken as an estimate of T_g from BLS measurements. Curves for samples in which KET exceeds the solubility limit significantly deviate from the master curve and, more importantly, their profile can be reproduced reasonably well by a linear combination of the derivative profile of pure amorphous KET and of the sample with 25 % of KET **(Figure 5B)**. Therefore, the BLS frequency keeps track separately of T_g of the PLGA/KET homogeneous mixture (KET-saturated PLGA) and of the amorphous KET domains dispersed in the matrix, thus confirming the biphasic amorphous composition of PLGA loaded with KET > 25% (w/w).

The comparison between the T_g values obtained from DSC **(Table S1) and BLS (Table S3)** is shown in **Figure 6A**. PLGA plasticization with increasing KET content is clearly confirmed by BLS, although slightly lower T_g values were recorded (ΔT_g □ -4 °C in all PLGA-containing samples). In this regard, it is well known that the absolute value of T_g depends on the thermomechanical history of the sample and on the heating/cooling rate employed to perform the measurements (Correira et al., 2000). Since all the samples went through a thermal treatment to erase the thermo-mechanical history, the observed difference should be reasonably explained by the lower cooling rate (1 °C/min instead of 10 °C/min) used in the BLS experiment. Indeed, a measure of T_g as a function of the heating rate in pure KET, PLGA and two different polylactic acid samples **(Figure 6B)**, indicates that a rate

change from 10 to 1 °C/min can account for a T_g reduction of about 4 °C. This reduces to zero (within the experimental uncertainty) the difference between the T_g that would be obtained from the two techniques at equal heating rate in all the samples, with the exception of pure KET **(Figure 6C)**. Indeed, T_g values directly measured in KET by DSC and BLS using the same heating rates (1 °C/min and 10 °C/min) maintain a difference of 4 °C, with BLS giving a lower T_g **(Figure 6A)**. This discrepancy remains an intriguing issue. It should be noted, however, that the glass transition phenomenon can be observed with many different techniques and these, by probing the dynamics through different physical properties, may provide slightly different results in terms of T_g. Differences in the range of ±5 °C were recently reported by comparing the results obtained with five different experimental techniques (including BLS) and *ab initio* simulations (Ruggiero et al., 2017).

The high sensitivity of the BLS frequency to T_g is further demonstrated in **Figure 7**, by comparing the quantity -df/dT vs. T at different heating and cooling rates for pure KET, as an exemplary case. It is interesting to note that the profile of -df/dT is closely reminiscent of a calorimetric thermogram dH/dT obtained by cooling/heating across the T_g, suggesting that the frequency of longitudinal acoustic modes is changing in strict response to enthalpy changes. In particular, two effects that are usually observed in DSC data are clearly reproduced in temperature scanning BLS data: i) the rate dependence of T_g and ii) an overshoot in the heating scan due to enthalpic relaxation.

3.3. Molecular dynamics

Numerical simulations were performed to shed light on the nature of PLGA/KET interactions established during the formation of PLGA/KET homogeneous mixtures (i.e., solid solutions) and PLGA plasticization.

The first part of the computational study evaluated the effect of heating on the conformational behaviour of the PLGA bundle when inserted in the apolar CCl_4 solvent. The profiles of the end-toend distance reveal that the PLGA chains retained a rather extended conformation at ~ 22 °C (295

K), a temperature below the measured PLGA T_g, while the PLGA chains tended to assume more folded geometries for temperatures roughly corresponding to or above T_g **(Figure S2A)**. Notably, the three simulations performed at higher temperatures (i.e., 335, 375, and 415 K) reveal very similar behaviours, thus suggesting that the folding degree does not increase progressively with heating but has an almost constant increase when the temperature rises above T_g (**Figure S2A**). Despite the increase in folded geometries, heating induced a slight increase of the interaction surface between polymer and CCl_4, a result that can be explained by considering that the PLGA folded conformations induce a worsening in the interactions that stabilize the PLGA bundle **(Figure S2B)**.

The obtained results suggest that the PLGA conformational behaviour markedly changes above T_g showing a clear increase of the folded geometries, while the extended helical conformations appear reasonably stable only at colder temperatures. Such a conformational shift induces a limited increase in the surface accessibility of the polymer mostly ascribable to a partial unpacking of the PLGA bundle.

In the second part of the computational study, 850 KET molecules were used to solvate the PLGA bundle (six 16-mers) obtained in the previous MD runs, at the same temperatures. The dynamic profile of the interaction surfaces shows that the PLGA/KET interactions progressively increased with heating, showing significant differences between 295 and 335 K as well as between 335 and 375 K, and less pronounced differences between 375 and 415 (particularly in the second part of the MD run). This suggests that the simulated system tended to reach a sort of plateau above 375 K (**Figure 8A**). A similar behaviour was shown by the number of intermolecular contacts between PLGA and KET, encoded by the number of KET molecules found in a 3 Å layer around the PLGA oligomers. The KET density around PLGA molecules markedly increased with heating and, similarly to what reported above, the greatest differences observed when comparing the results at 375 K with those obtained in the colder systems **(Figure 8B)**.

To gain further information on the effect of heating on the PLGA/KET interactions, **Figure 9** reports the radial pair distribution function, *g*(r), of the interatomic distances between the O atoms of PLGA oligomers and KET molecules **(Figure 9A)** and between the C atoms of PLGA oligomers and KET molecules **(Figure 9B)**. The former is representative of polar interactions and, in particular, of the H-bonds between the KET carboxyl function and the PLGA ester groups, while the latter encodes for non-polar contacts, including Van der Waals contacts between hydrophobic atoms and π-π stacking interactions between KET aromatic rings and PLGA ester functions. The radial pair distribution functions reveal that the polar contacts clearly decreased with heating and this effect was particularly relevant at 415 K where the peak corresponding to H-bonds (between 1.8 and 3 Å) roughly disappeared **(Figure 9A)**. In contrast, the non-polar contacts increased upon heating and the differences were particularly evident in the region between 4.5 and 5.5 Å that should correspond to π-π stacking interactions **(Figure 9B)**. In particular, the largest increase was found between 335 K and 375 K and a more reduced between 375 K and 415 K.

When considering the hydrophobic nature of PLGA, one may conclude that at the three lower temperatures the gain in non-polar contacts exceeds the weakening of the H-bonds and a general reinforcement of the PLGA/KET interactions is produced by heating. In contrast, the marked reduction of polar interactions at 415 K is at most counterbalanced by a modest increase in apolar contacts, and the PLGA/KET interactions remain almost constant. In fact, the number of KET molecules at a distance of 6 Å from the surface of PLGA oligomers, the most prone to perform interactions, increase with temperature even if H-bonding decreases **(Figure 10)**.

Overall, MD simulations suggest that heating induces a reinforcement of the PLGA/KET interactions at most up to 375 K, with negligible further changes at the highest simulated temperature. Such reinforcement is primarily driven by an enhancement of non-polar interactions. This enthalpic effect favourably contributes to the increased solubility that was suggested by the transparency change and

detected in the BLS experiment. On the other hand, entropic effects also contribute to the phase-stability of the system.

It is interesting to note that the interaction surfaces of PLGA with CCl4 and KET are very similar, thus suggesting that PLGA conformational changes can be attributed almost entirely to heating, regardless of the solvent environment.

3.4. Concluding remarks

KET interacts with PLGA by exerting a plasticizing effect that reaches a maximum around weight fractions of 0.25. Above this amount, KET forms a second phase in the plasticized matrix that, depending on the production method, can be crystalline or amorphous. This highlights the crucial role of the preparation method in determining the physical state of the generated system.

Concerning the KET plasticizing effect, it is reasonable that the interactions responsible for the T_g reduction, as well as for the limited solubility, are H-bonds established between the KET carboxylic group and PLGA ester groups. It seems that, at room temperature, PLGA can solubilize 25% (w/w) of KET that, barely, corresponds to 1 KET molecule every 12 ester groups, far from the ideal situation of 1 KET molecule per ester group. Obviously, entanglement of PLGA polymer chains and steric hindrance of KET molecules prevent this situation from being realized. MD simulations show that at low temperatures more KET molecules around PLGA are prone to establish H-bonds, while at higher temperatures the number of KET molecules around PLGA increases although their probability to establish H-bonds decreases **(Figure 11)**. As BLS and MD simulations results suggest that KET solubility increases with temperature, it is speculated that H-bonds are not the only interactions involved in PLGA/KET solubility but that non-polar interactions might be responsible for the solubility enhancement with increasing temperature.

Also, we have demonstrated that BLS spectroscopy, used in the temperature scanning mode, is a powerful technique able: (i) to probe the glass transition phenomenon, as the quantity $-df/dT$ *vs* T closely matches the behaviour of dH/dT obtained by DSC; (ii) to discriminate the physical state of the drug embedded in the polymer matrix, as the BLS frequency *vs* T keeps track separately of the glass transition of KET-saturated PLGA and of amorphous KET confined into the matrix; and iii) to individuate the drug solubility limit in the polymer matrix, as the multiple scattering effects associated to sample heterogeneity give rise to broadening of the BLS spectra.

Acknowledgements

The authors acknowledge the technical support of the laboratory LUNA (Laboratorio Universitario di Nanomateriali) of the University of Perugia and in particular the contribution of Alessandro Di Michele for SEM analyses.

References

Alexis, F., 2005. Factors affecting the degradation and drug-release mechanism of poly (lactic acid) and poly [(lactic acid)-co-(glycolic acid)]. Polym. Int. 54, 36-46.

Blasi, P., 2019. Poly(lactic acid)/poly(lactic-co-glycolic acid)-based microparticles: an overview. J. Pharm. Investig. 49, 337-346.

Blasi, P., Schoubben, A., Giovagnoli, S., Perioli, L., Ricci, M., Rossi. C., 2007. Ketoprofen poly(lactide-coglycolide) physical interaction. AAPS PharmSciTech 8 (2), article 37.

Briard, P.P., Rossi, J.C.,1990. Kétoprofène. Acta Crystallogr. C 46, 1036-1038.

Castiglia, S.R.V., Fioretto, D., Verdini, L., Samios, D., 2001. Network formation studied by temperature scanning brillouin scattering and differential scanning calorimetry techniques. II. J. Polym. Sci. Pol. Phys. 39, 1326-1336.

Corezzi, S., Comez, L., Zanatta, M., 2018. A simple analysis of Brillouin spectra from opaque liquids and its application to aqueous suspensions of poly-N-isopropylacrylamide microgel particles. J. Mol. Liq. 266, 460-466.

Correira, N.T., Alvarez, C., Moura Ramos, J.J., Descamps, M., 2000. Molecular motions in molecular glasses as studied by thermally stimulated depolarisation currents (TSDC). Chem. Phys. 252, 151-163.

Crowley, P., Martini, L., 2001. Drug-excipient interaction. Pharm. Technol. 13, 26-34.

Debotton, N., Dahan, A., 2017. Applications of polymers as pharmaceutical excipients in solid oral dosage forms. Med. Res. Rev. 37, 52-97.

Di Martino, P., Joiris, E., Gobetto, R., Masic, A., Palmieri, G.F., Martelli, S., 2004. Ketoprofenpoly(vinylpyrrolidone) physical interaction. J. Cryst. Growth. 265, 302-308.

Fernández-Carballido, A., Herrero-Vanrell, R., Molina-Martınez, I.T., Pastoriza, P., 2004. Biodegradable ibuprofen-loaded PLGA microspheres for intraarticular administration. Effect of labrafil addition on release in vitro. Int. J. Pharm. 279, 33-41.

Fioretto, D., Comez, L., Socino, G., Verdini, L., Corezzi, S., Rolla, P.A., 1999. Dynamics of density fluctuations of a glass-forming epoxy resin revealed by Brillouin light scattering. Phys. Rev. E. 59, 18991907.

Gasmi, H., Danede, F., Siepmann, J., Siepmann, F., 2015. Does PLGA microparticle swelling control drug release? New insight based on single particle swelling studies. J. Control. Release. 213, 120-127.

Gasteiger, J., Marsili, M., 1978. A new model for calculating atomic charges in molecules. Tetrahedron Lett. 19, 3181-3184.

Gue, E., Muschert, S., Willart, J.F., Danede, F., Delcourt-Debruyne, E., Descamps, M., Siepmann J., 2015. Accelerated ketoprofen release from spray-dried polymeric particles: importance of phase transitions and excipient distribution. Drug. Dev. Ind. Pharm. 41, 838-850.

Gue, E., Willart, J.F., Muschert, S., Danede, F., Delcourt, E., Descamps, M., Siepmann J., 2013. Accelerated ketoprofen release from polymeric matrices: importance of the homogeneity/heterogeneity of excipient distribution. Int. J. Pharm. 457, 298-307.

Guo, Y., Yang, Y., He, L., Sun, R., Pu, C., Xie, B., He, H., Zhang, Y., Yin, T., Wang, Y., Tang, X., 2017. Injectable sustained-release depots of PLGA microspheres for insoluble drugs prepared by hot-melt extrusion. Pharm. Res. 34, 2211-2222.

Hancock, B.C., Zografi, G., 1991. Characteristics and significance of the amorphous state in pharmaceutical systems. J. Pharm. Sci. 86, 1-12.

Kamaly, N., Yameen, B., Wu, J., Farokhzad, O.C., 2016. Degradable controlled-release polymers and polymeric nanoparticles: Mechanisms of controlling drug release. Chem Rev. 116, 2602-2663.

Kawakami, K., 2019. Crystallization tendency of pharmaceutical glasses: Relevance to compound properties, impact of formulation process, and implications for design of amorphous solid dispersions. Pharmaceutics. 11, 202.

Knopp, M.M., Tajber, L., Tian, Y., Olesen, N.E., Jones, D.S., Kozyra, A., Löbmann, K., Paluch, K., Brennan, C.M., Holm, R., Healy, A.M., Andrews, G.P., Rades, T., 2015. Comparative study of different methods for the prediction of drug-polymer solubility. Mol. Pharm. 12, 3408-3419.

Korb, O., Stützle, T., Exner, T.E., 2009. Empirical scoring functions for advanced protein-ligand docking with PLANTS. J. Chem. Inf. Model. 49, 84-96.

Kunze, C., Freier, T., Kramer, S., Schmitz, K.P., 2002. Anty-inflammatory prodrugs as plasticizers for biodegradable implant materials based on poly (3-hydroxybutyrate). J. Mater. Sci. 13, 1051-1055.

Lange, J., de Souza, F.G., Nele, M., Tavares, F.W., Segtovich, I.S.V., da Silva, G.C.Q., Pinto, J.C., 2016. Molecular dynamic simulation of oxaliplatin diffusion in poly(lactic acid-co-glycolic acid). Part A: parameterization and validation of the force-field CVFF. Macromol. Theory Simul., 25, 45-62.

Liechty, W.B., Kryscio, D.R., Slaughter, B.V., Peppas, N.A., 2010. Polymers for drug delivery systems. Ann. Rev. Chem. Biomol. Eng. 1, 149-173.

Lim, S.H., Kathuria, H., Tan, J.J.Y., Kang, L., 2018. 3D printed drug delivery and testing systems – a passing fad or future? Adv. Drug Deliver. Rev. 132, 139-168.

Ngai, K.L., 2007a. J. Non-Cryst. Solids. 353, 709-718.

Ngai, K.L., 2007b. All standard theories and models of glass transition appear to be inadequate: missing some essential physics, in: Rzoska, S.J., Mazur, V.A. (Eds.) Soft Matter under Exogenic Impacts. NATO Science Series II: Mathematics, Physics and Chemistry, vol 242. Springer, Dordrecht, pp. 91-111.

Papkov, V.S., Nikiforova, G.G., Nikol'sky, V.G., Krasotkina, I.A., Obolonkova, E.S., 1998. Transparent microheterogeneous blends containing a multiblock copolymer and a foreign homopolymer. Polymer. 39, 631-640.

Pedretti, A., Villa, L., Vistoli, G., 2002. VEGA: a versatile program to convert, handle and visualize molecular structure on Windows-based PCs. J. Mol. Graph. Model. 21, 47-49.

Phillips, J.C., Braun, R., Wang, W., Gumbart, J., Tajkhorshid, E., Villa, E., Chipot, C., Skeel, R.D., Kalé, L., Schulten, K., 2005. Scalable molecular dynamics with NAMD. J. Comput. Chem. 26, 1781-1802.

Qian, F., Huang, J., Hussain M.A., 2010. Drug-polymer solubility and miscibility: Stability consideration and practical challenges in amorphous solid dispersion development. J. Pharm. Sci. 99, 2941-2947.

Ricci, M., Blasi, P., Giovagnoli, S., Rossi, C., Macchiarulo. G., Luca, G., Basta, G., Calafiore, R., 2005. Ketoprofen controlled release from composite microcapsules for cell encapsulation: effect on posttransplant acute inflammation. J. Control. Release. 107, 395-407.

Ruggiero, M.T., Krynski, M., Kissi, E.O., Sibik, J., Markl, D., Tan, N.Y., Arslanov, D., van der Zande, W., Redlich, B., Korter, T.M., Grohganz, H., Löbmann, K., Rades, T., Elliott, S.R., Zeitler, J.A., 2017. The significance of the amorphous potential energy landscape for dictating glassy dynamics and driving solidstate crystallization. Phys. Chem. Chem. Phys. 19, 30039-30047.

Schoubben, A., Ricci, M., Giovagnoli, S., 2019. Meeting the unmet: from traditional to cutting-edge techniques for poly lactide and poly lactide-co-glycolide microparticle manufacturing. J. Pharm. Investig. 49, 381-404.

Selmin, F., Blasi, P., DeLuca, P.P., 2012. Accelerated polymer biodegradation of risperidone poly(D, Llactide-co-glycolide) microspheres. AAPS PharmSciTech. 13, 1465-1472.

Siegel, S.J., Kahn, J.B., Metzger, K., Winey, K.I., Werner, K., Dan, N., 2016. Effect of drug type on the degradation rate of PLGA matrices. Eur. J. Pharm. Biopharm. 64, 287-293.

Stewart, J.J., 2013. Optimization of parameters for semiempirical methods VI: more modifications to the NDDO approximations and re-optimization of parameters. J. Mol. Model. 19, 1-32.

Tarvainem, M., Sutinen, R., Somppi, M., Paronem, P., Poso, A., 2001. Predicting plasticization efficiency from three-dimensional molecular structure of a polymer plasticizer. Pharm. Res. 18, 1760-1766.

Ueda, H., Aikawa, S., Kashima, Y., Kikuchi, J., Ida, Y., Tanino, T., Kadota, K., Tozuka, Y., 2014. Antiplasticizing effect of amorphous indomethacin induced by specific intermolecular interactions with PVA copolymer. J. Pharm. Sci. 103:2829-2838.

Wahab, M.A., Kim, I., Ha, C-S., 2003. Microstructure and properties of polyimide/poly(vinylsilsesquioxane) hybrid composite films. Polymer. 44, 4705-4713.

Wu, C., McGinity, J.W., 1999. Non-traditional plasticization of polymeric films. Int. J. Pharm. 177, 15-27.

Wu, C., McGinity, J.W., 2001. Influence of Ibuprofen as a solid-state plasticizer in Eudragit® RS 30 D on the physicochemical properties of coated beads. AAPS PharmSciTech. 2, 35-43.

Figure captions

Figure 1. DSC data (exo up) of the second heating ramp of (from top to bottom): PLGA RG 504, PLGA films containing different amounts of KET (% w/w), and pure KET.

Figure 2. Three-dimensional SEM images of the upper surface of PLGA films containing different amounts of KET. Please note that KET 0% and KET 100% are pure PLGA and pure KET, respectively.

Figure 3. BLS spectra of PLGA loaded with 25% (w/w) of KET, during a temperature scan from 120 °C to -60 °C performed at a cooling rate of 1 °C/min.

Figure 4. (A) Comparison between BLS spectra of PLGA/KET samples with 25% and 50% (w/w) of KET at 100 °C and -20 °C. (B) Temperature dependence of the BLS linewidth in PLGA/KET samples with 35% and 50% (w/w) of KET. Solid symbols represent the parameter Γ obtained from the fit with Eq.1 (see text); open symbols represent the FWHM of the peaks directly estimated from the BLS spectra.

Figure 5. (A) Temperature dependence of the BLS frequency, *f*, of PLGA/KET samples with different amounts of KET (% w/w) see legend during cooling at 1 °C/min. Data for pure KET are reported as measured, those for the other samples are progressively shifted downward by 1 GHz, for clarity. For the monophasic samples, an arrow indicates the value of T_g measured by DSC. (B) Rate of variation with temperature of the BLS frequency, –d*f*/dT, of all the mixtures. For the monophasic samples, T_g^{BLS} is estimated as the midpoint temperature of the jump in the data. Bold solid lines (in blue and orange) reconstruct the derivative profile of the samples with 35% and 50% of KET as a linear combination of the derivative profiles of pure KET and of the KET-saturated PLGA sample (25% of KET). (C) Master curve of the quantity –d*f*/dT for the monophasic samples, obtained by shifting the temperature scale by T_g^{BLS} of each sample.

Figure 6. (A) T_g vs. KET content in PLGA/KET mixtures, as determined by DSC and BLS. (B) Heating rate dependence of T_g measured by DSC in KET, PLGA and two polylactic acid (PLA) samples. To facilitate comparison, the data for PLGA, PLA 202H and PLA 202S have been shifted, respectively, by -48, -49 and -42 °C. The difference between the values of T_g measured at 10°C/min

and 1°C/min in all these compounds is about 4 °C. (C) Difference between the T_g values measured at 10°C/min by DSC and at 1°C/min by BLS (solid symbols), and rate-corrected difference (open symbols).

Figure 7. Rate of variation with temperature of the BLS frequency, $-df/dT$, measured in pure KET during cooling and heating, at rates of 1 °C/min and 10 °C/min.

Figure 8. (A) Number of contacts between the PLGA bundle and the surrounding KET molecules, and (B) dynamic profile of their interaction surface.

Figure 9. Radial pair distribution function, $g(r)$, of the distances (A) between the O atoms of PLGA and KET molecules, and (B) between the C atoms of PLGA and KET molecules.

Figure 10. Mean number of KET molecules at a distance of 3, 6, 9 and 12 Å from the PLGA oligomers at different temperatures.

Figure 11. Arrangement of the six closest KET molecules around the first monomers of one PLGA oligomer, in the last frame of the MD runs at 295 K (A) and 375 K (B). Notice that at 295 K almost all the KET molecules (5 out of 6) expose their carboxyl group to the oligomer, while at 375 K only one KET molecule elicits H-bond between the carboxyl group and the PLGA ester function.

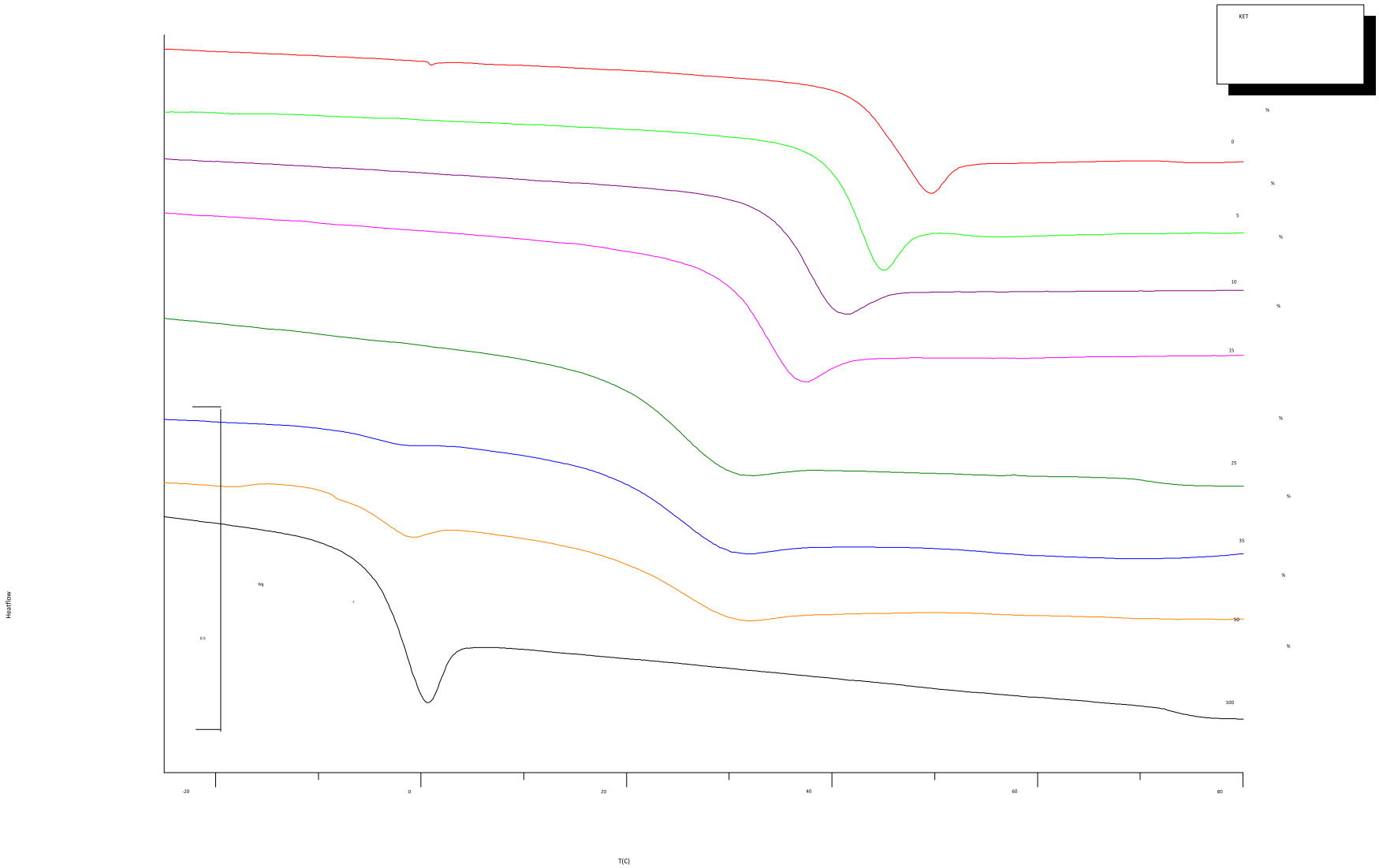
KET
%
0
%
5
%
10
%
15
%
25
%
35
%
50
%
100
Heatflow
W/g
0.5
-20
0
20
40
60
80
T(C)

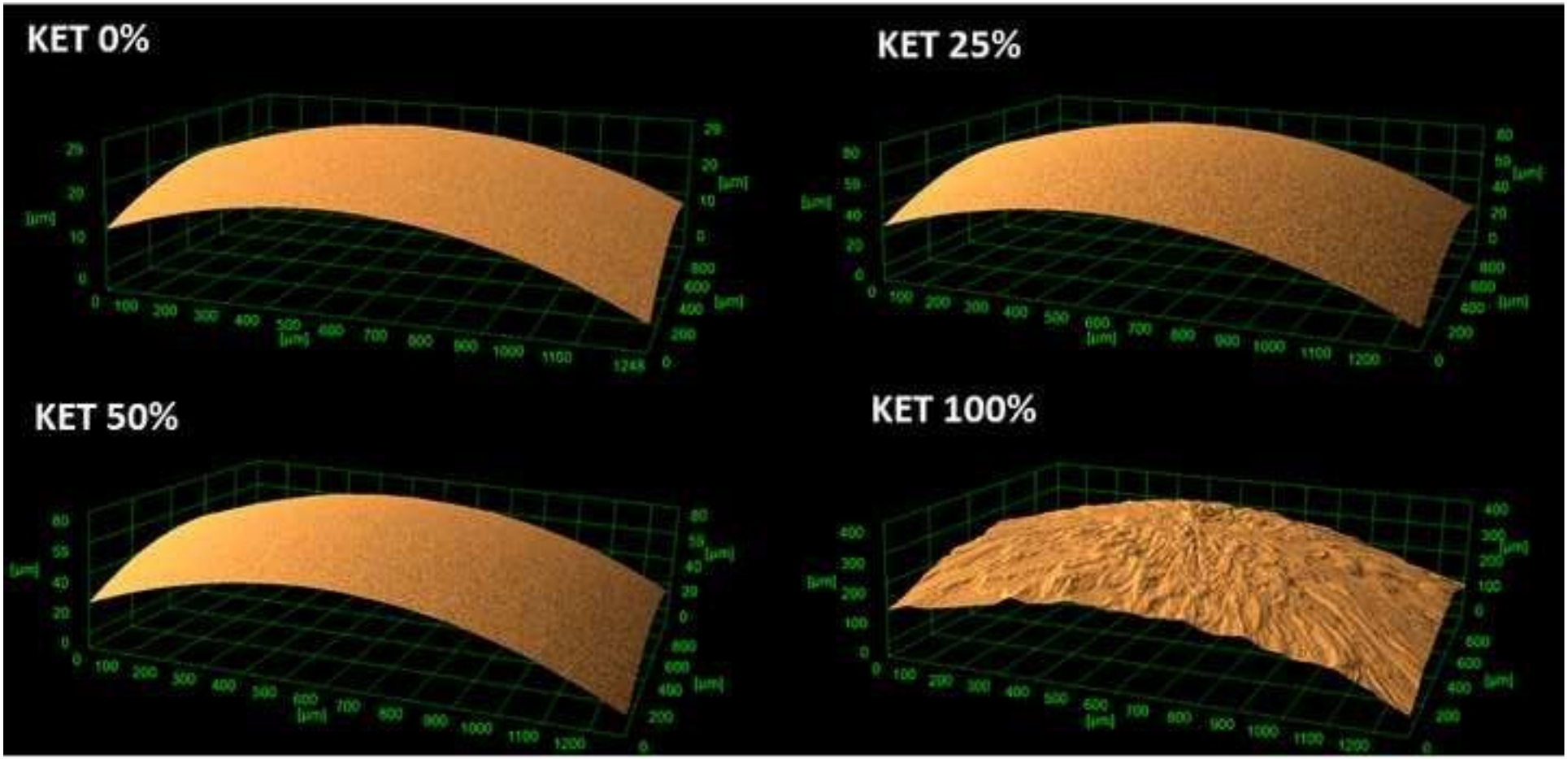
KET 0%
KET 25%
KET 50%
KET 100%

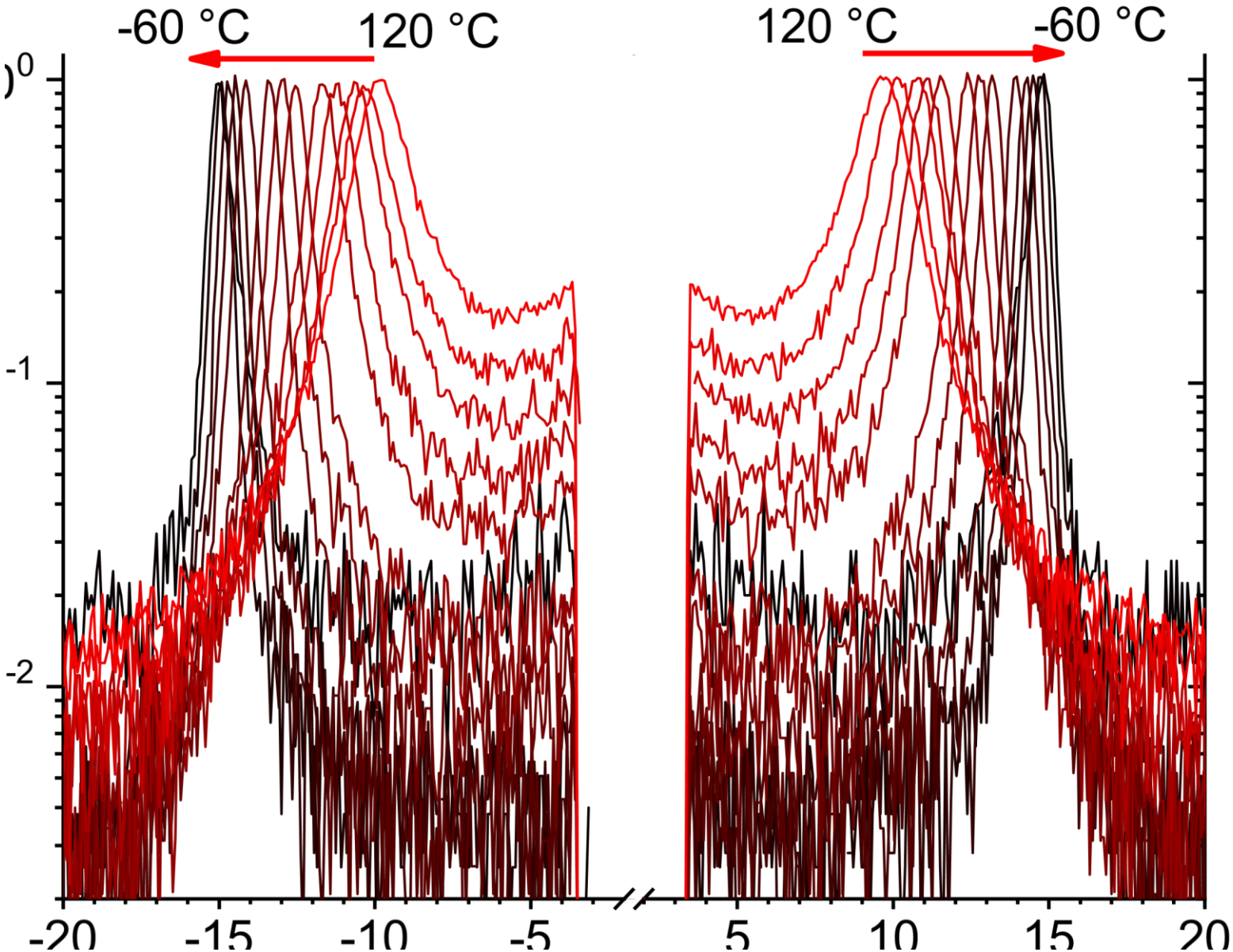
-60 °C
120 °C
120 °C
-60 °C
0
-1
-2
-20
-15
-10
-5
5
10
15
20

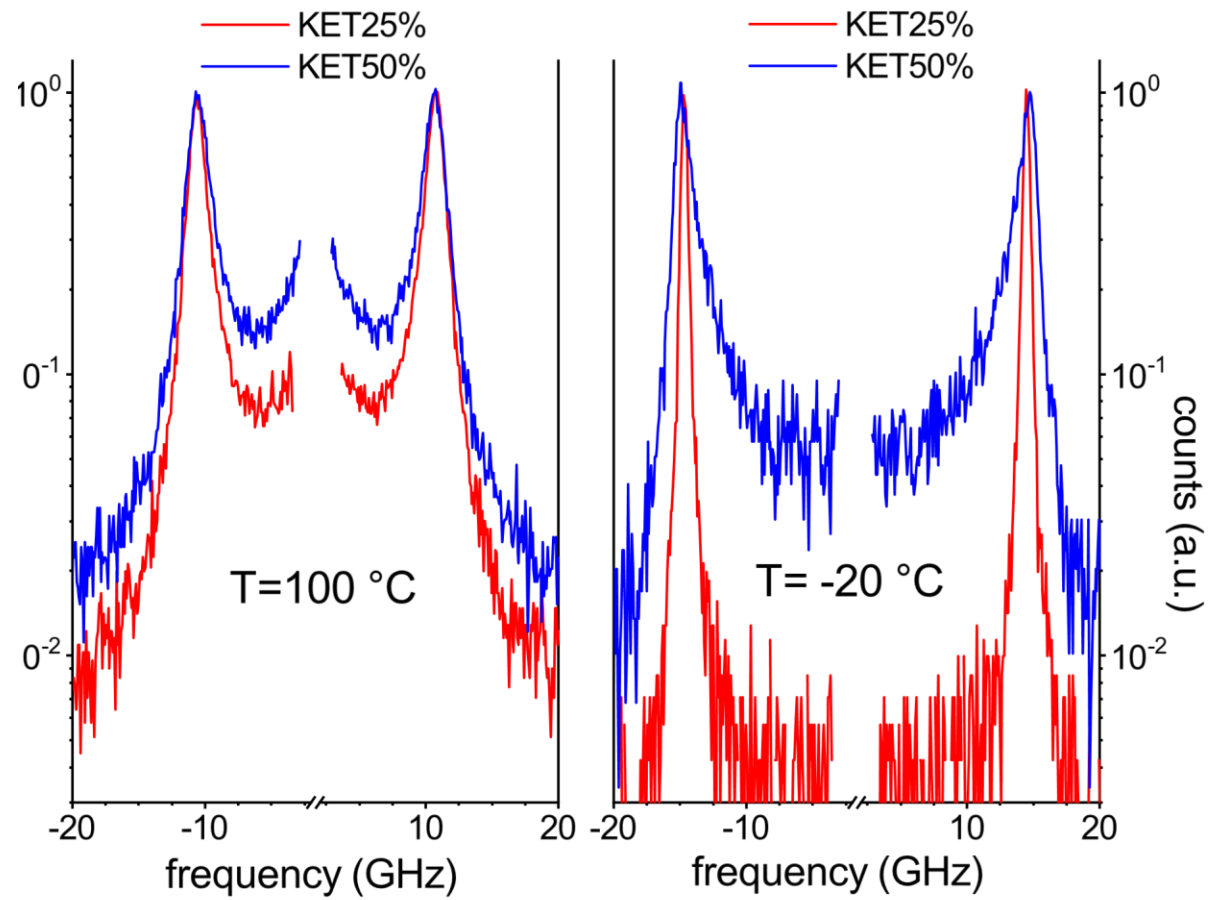
KET25%
KET50%
T=100 °C
T= -20 °C
frequency (GHz)
frequency (GHz)
counts (a.u.)

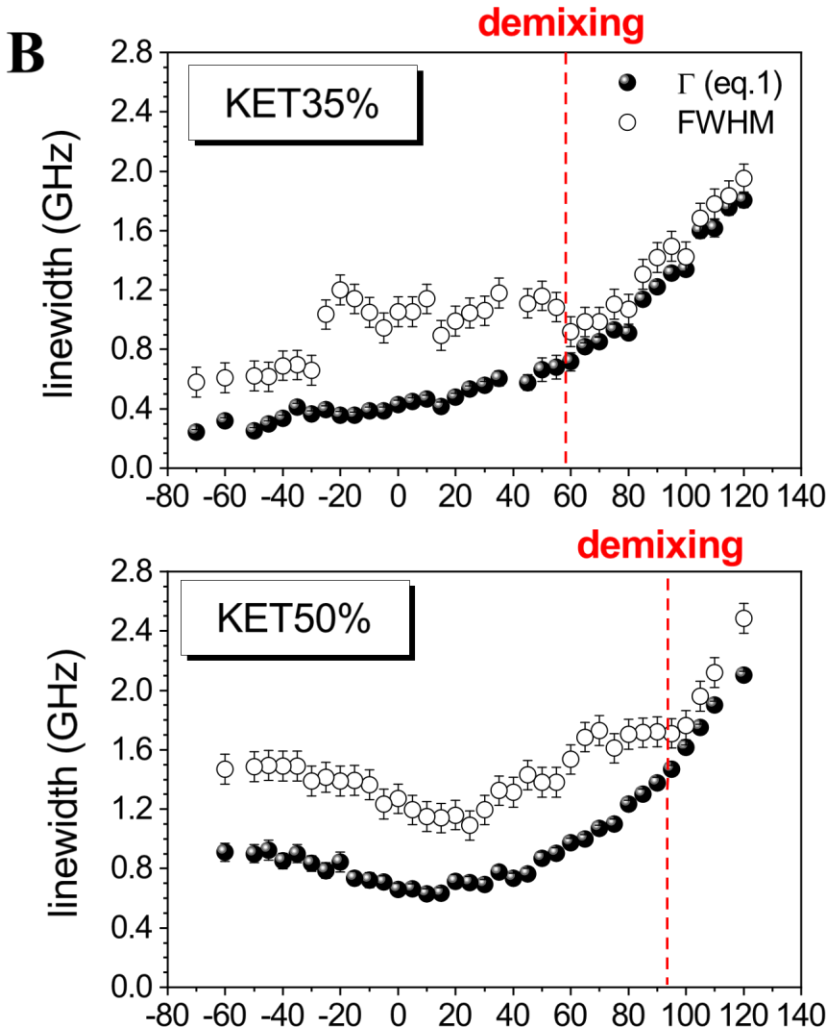
B
demixing
KET35%
Γ (eq.1)
FWHM
linewidth (GHz)
demixing
KET50%
linewidth (GHz)

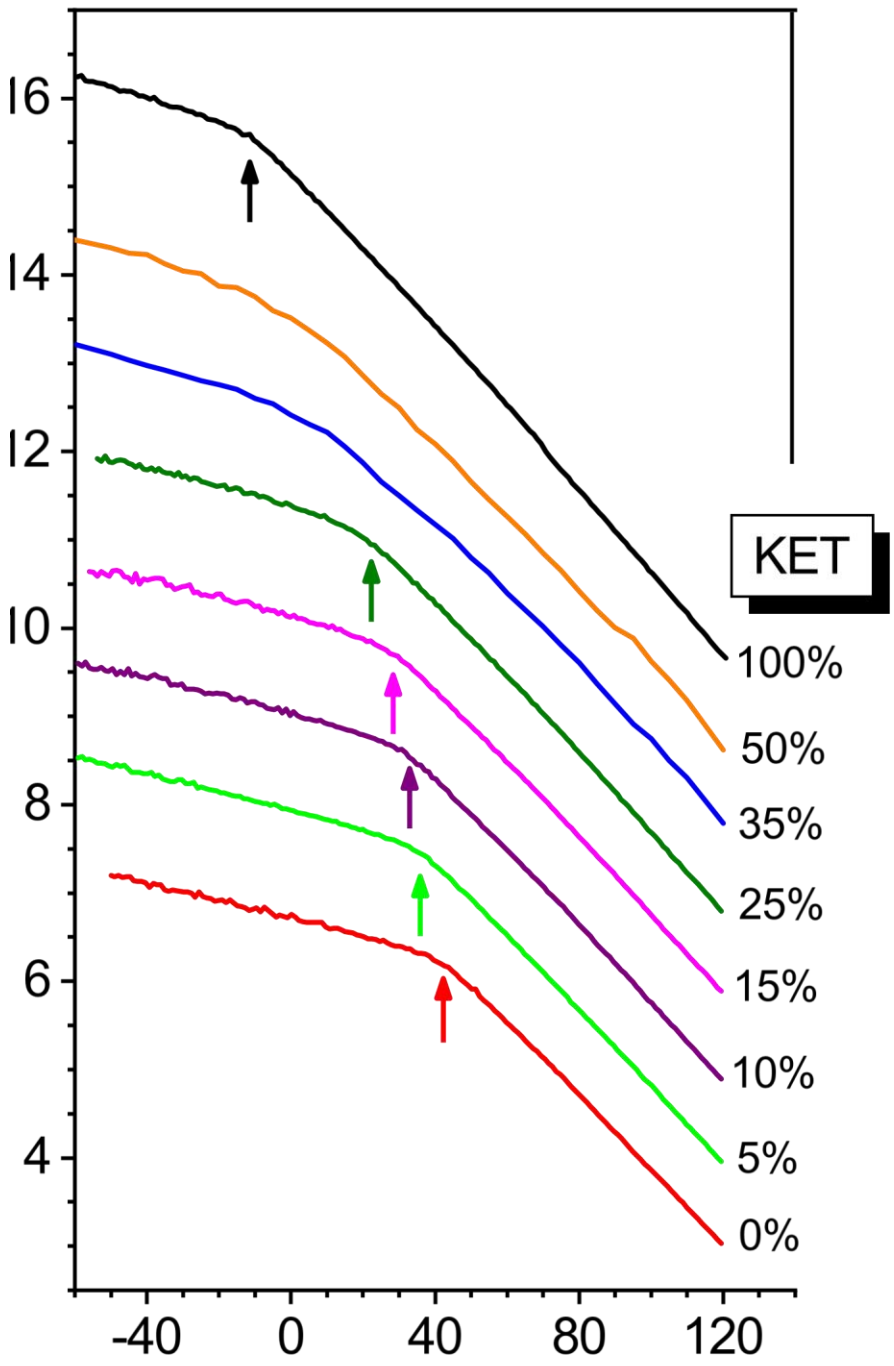
16
14
12
10
8
6
4
-40
0
40
80
120
KET
100%
50%
35%
25%
15%
10%
5%
0%

B

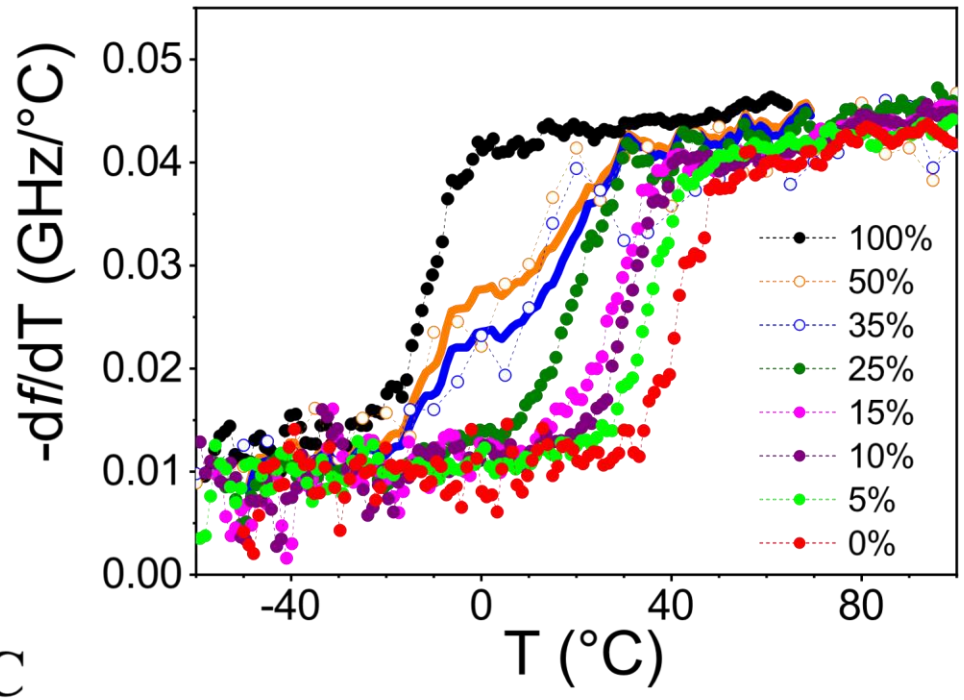
-df/dT (GHz/°C)
0.05
0.04
0.03
0.02
0.01
0.00
-40
0
40
80
T (°C)
100%
50%
35%
25%
15%
10%
5%
0%

C

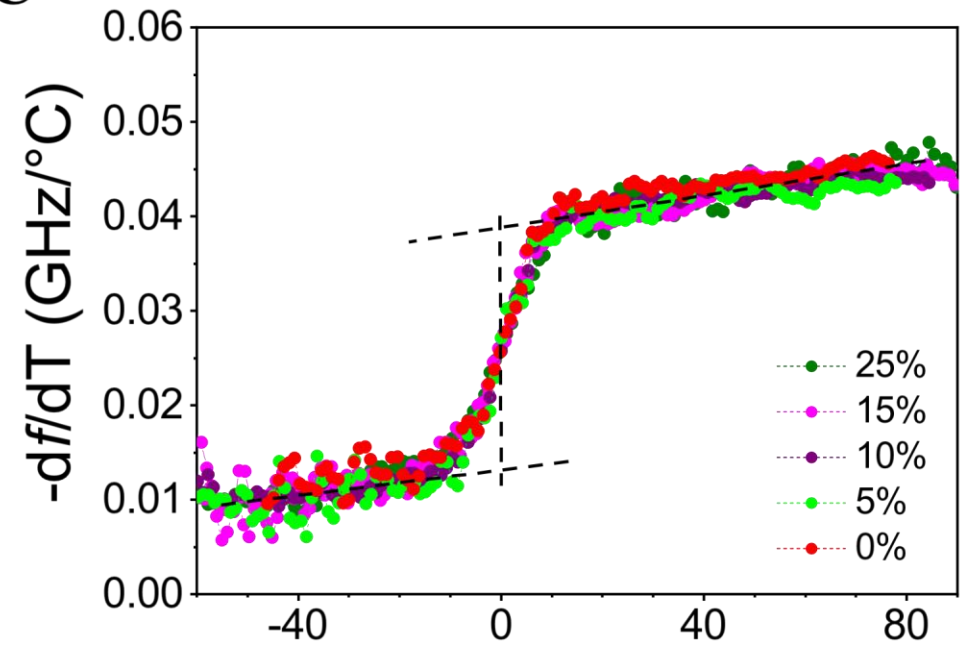
-df/dT (GHz/°C)
0.06
0.05
0.04
0.03
0.02
0.01
0.00
-40
0
40
80
25%
15%
10%
5%
0%

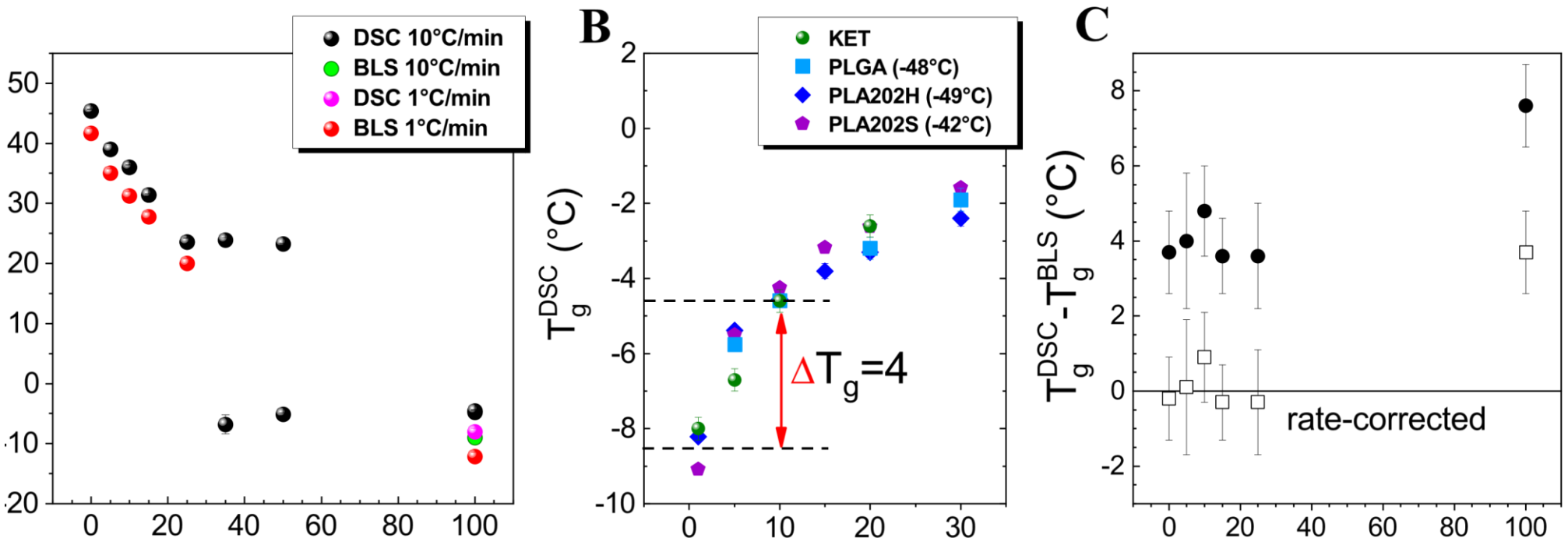
DSC 10°C/min
BLS 10°C/min
DSC 1°C/min
BLS 1°C/min
B
KET
PLGA (-48°C)
PLA202H (-49°C)
PLA202S (-42°C)
T_g^{DSC} (°C)
ΔT_g=4
C
T_g^{DSC}-T_g^{BLS} (°C)
rate-corrected

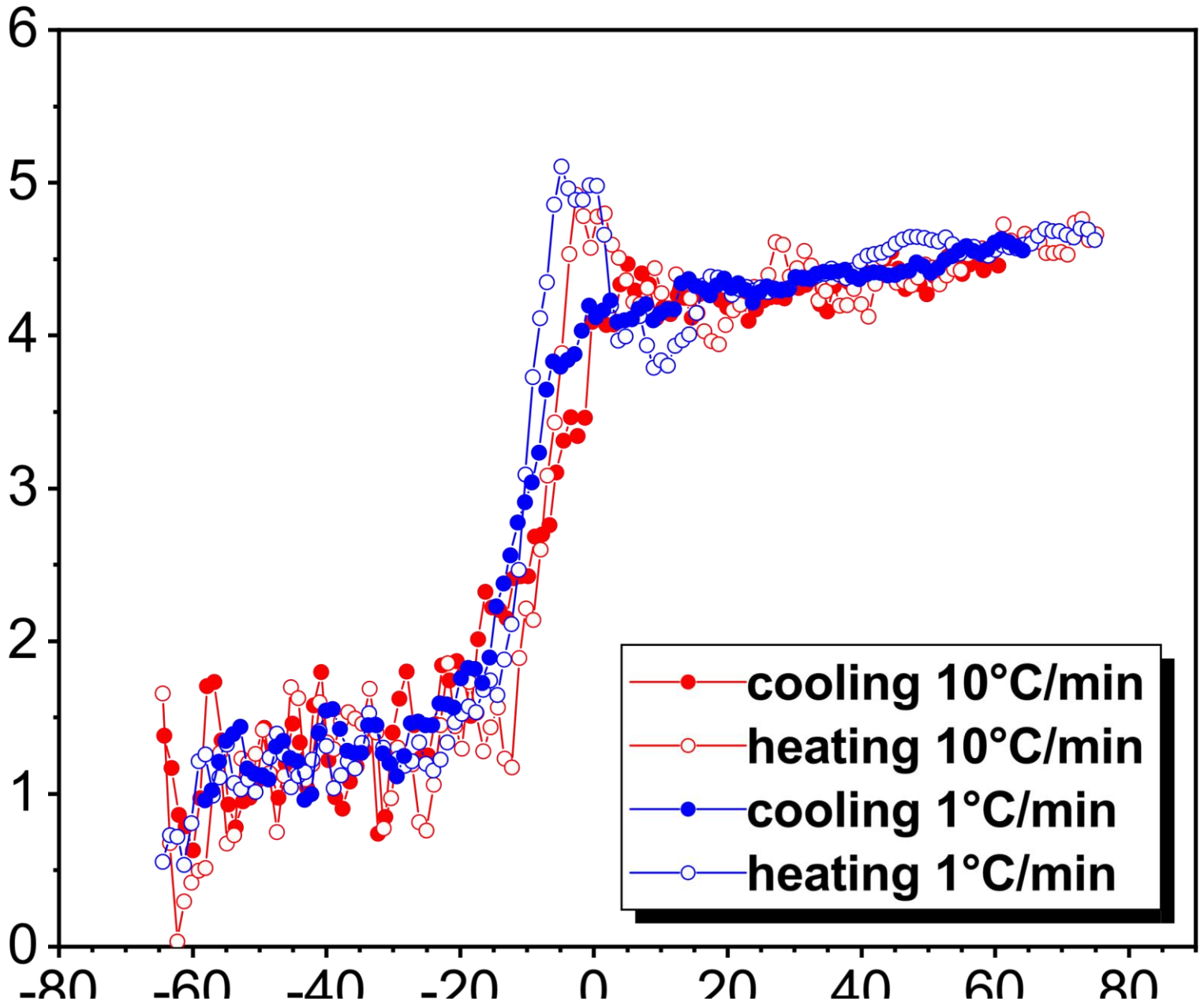
6
5
4
3
2
1
0
-80
-60
-40
-20
0
20
40
60
80
cooling 10°C/min
heating 10°C/min
cooling 1°C/min
heating 1°C/min

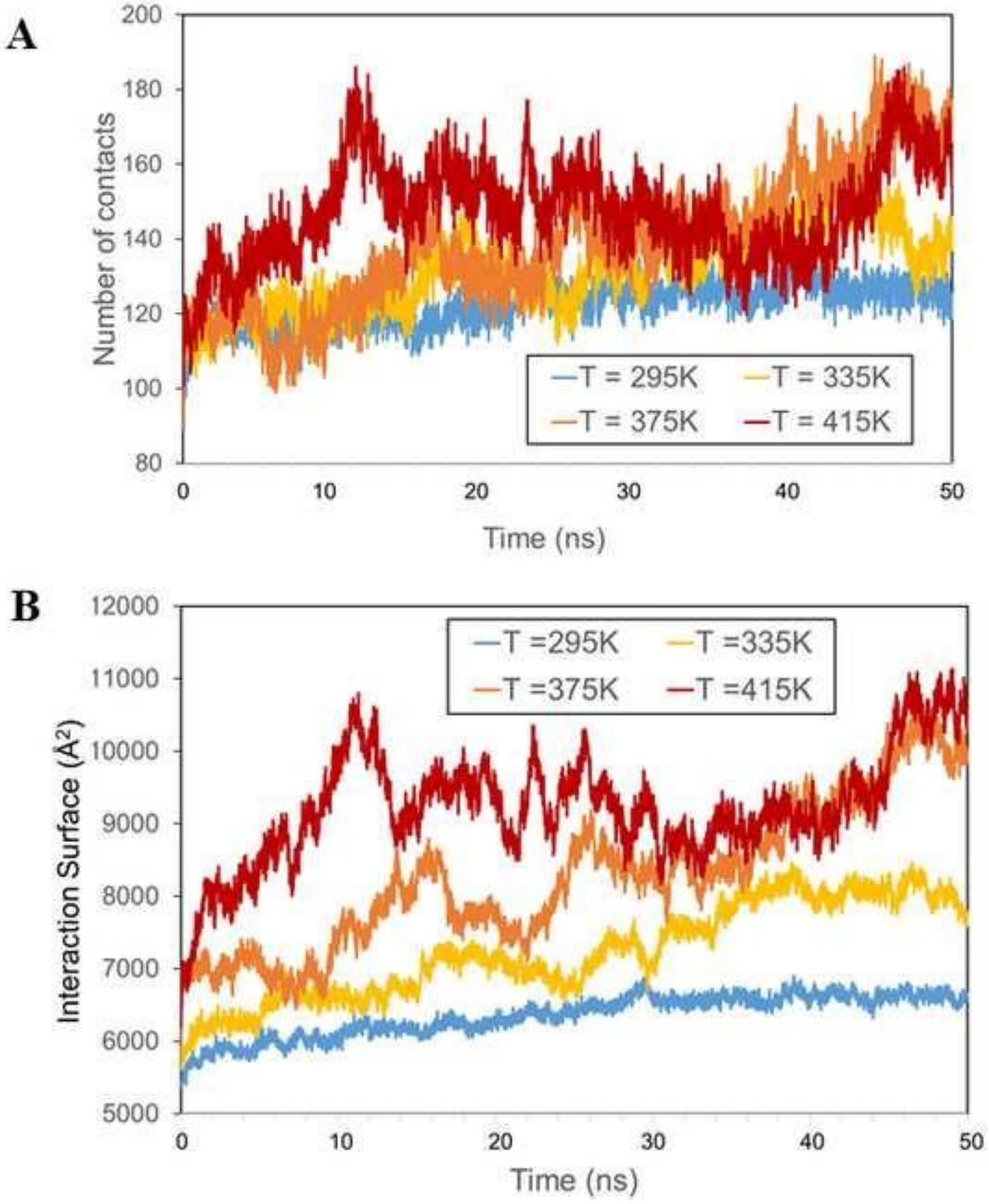
A
Number of contacts
200
180
160
140
120
100
80
0
10
20
30
40
50
Time (ns)
T = 295K
T = 335K
T = 375K
T = 415K
B
Interaction Surface (Å²)
12000
11000
10000
9000
8000
7000
6000
5000
0
10
20
30
40
50
Time (ns)
T =295K
T =335K
T =375K
T =415K

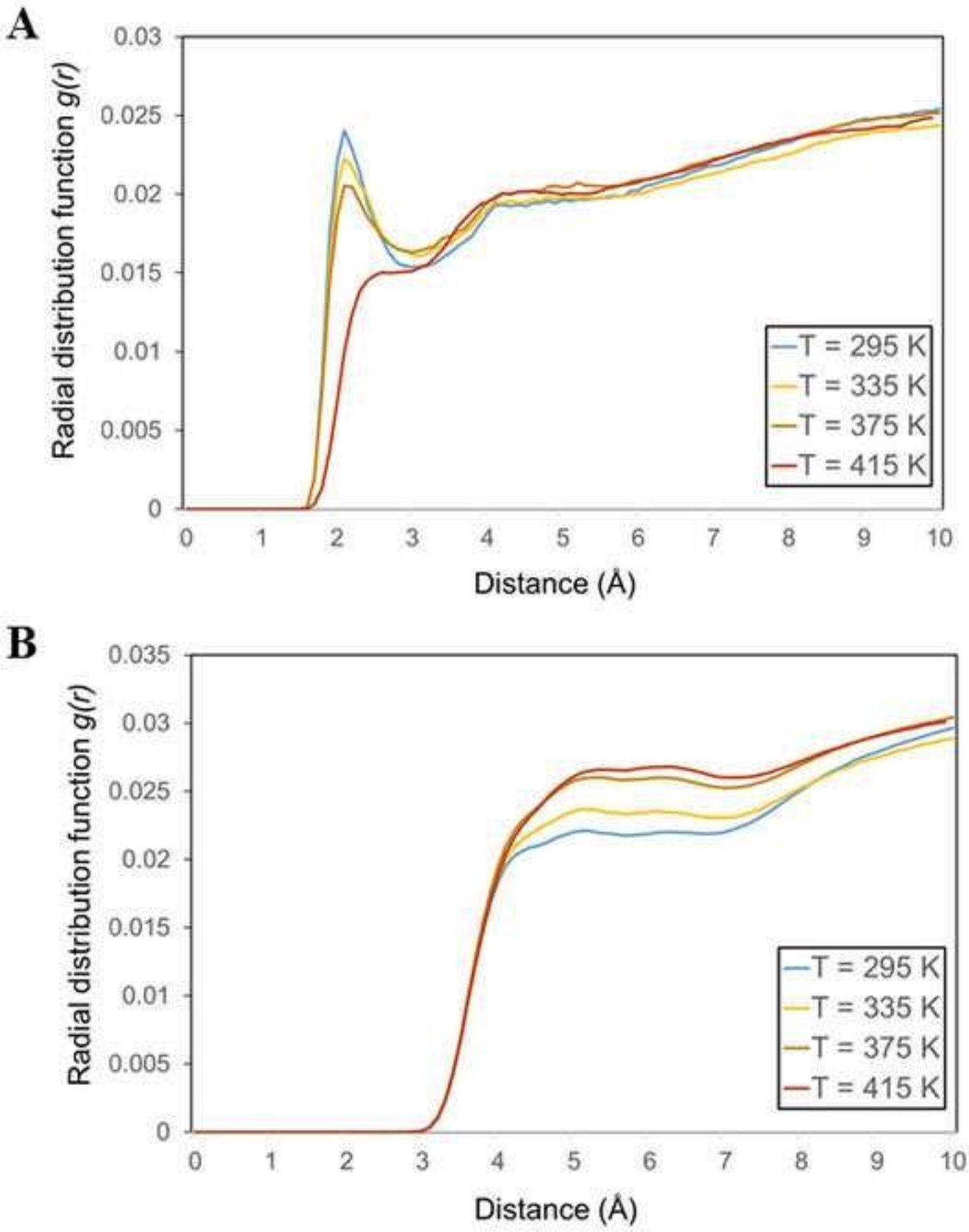
A
Radial distribution function g(r)
0.03
0.025
0.02
0.015
0.01
0.005
0
0 1 2 3 4 5 6 7 8 9 10
Distance (Å)
T = 295 K
T = 335 K
T = 375 K
T = 415 K
B
Radial distribution function g(r)
0.035
0.03
0.025
0.02
0.015
0.01
0.005
0
0 1 2 3 4 5 6 7 8 9 10
Distance (Å)
T = 295 K
T = 335 K
T = 375 K
T = 415 K

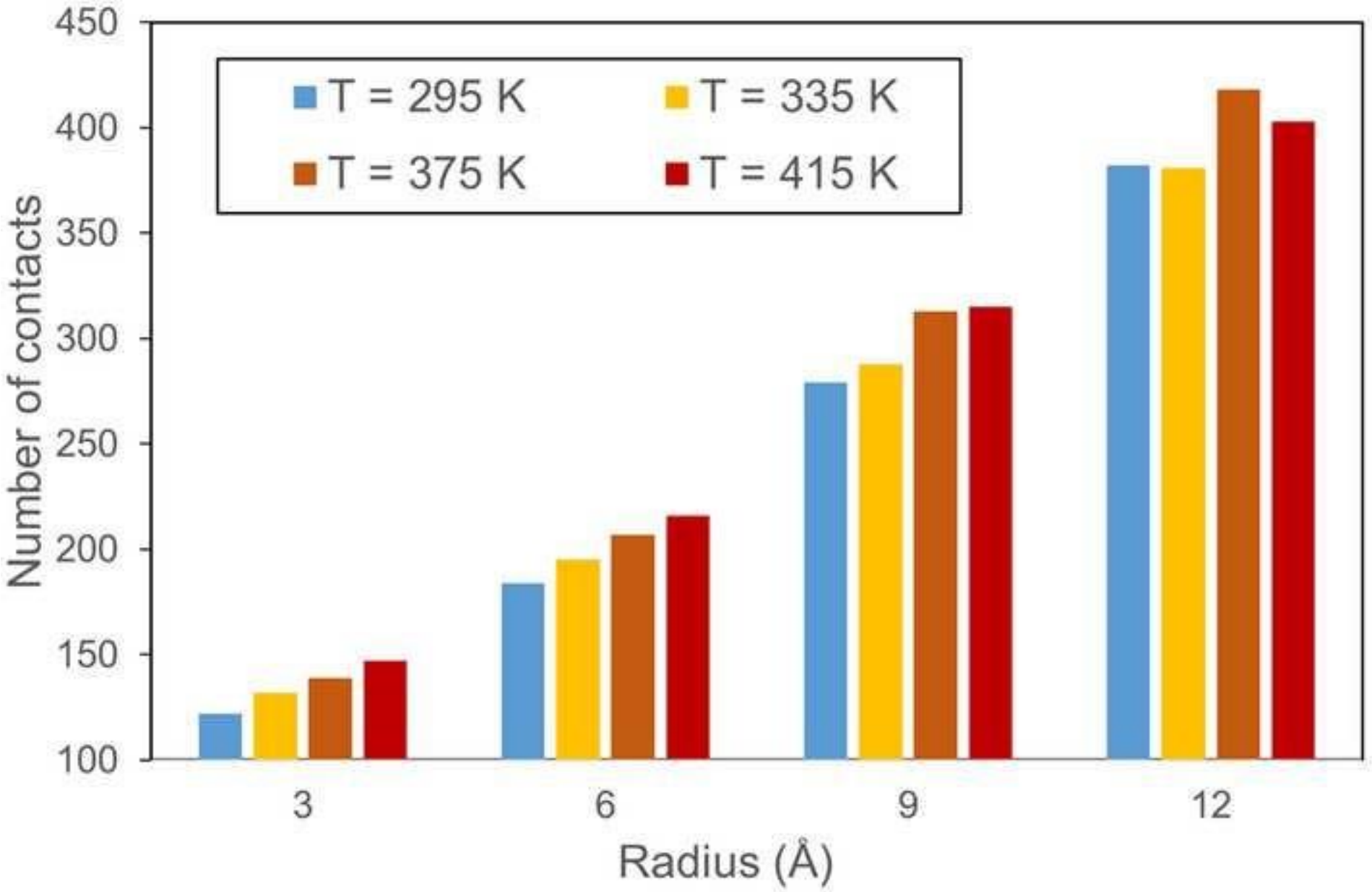
T = 295 K
T = 335 K
T = 375 K
T = 415 K
Number of contacts
450
400
350
300
250
200
150
100
3
6
9
12
Radius (Å)

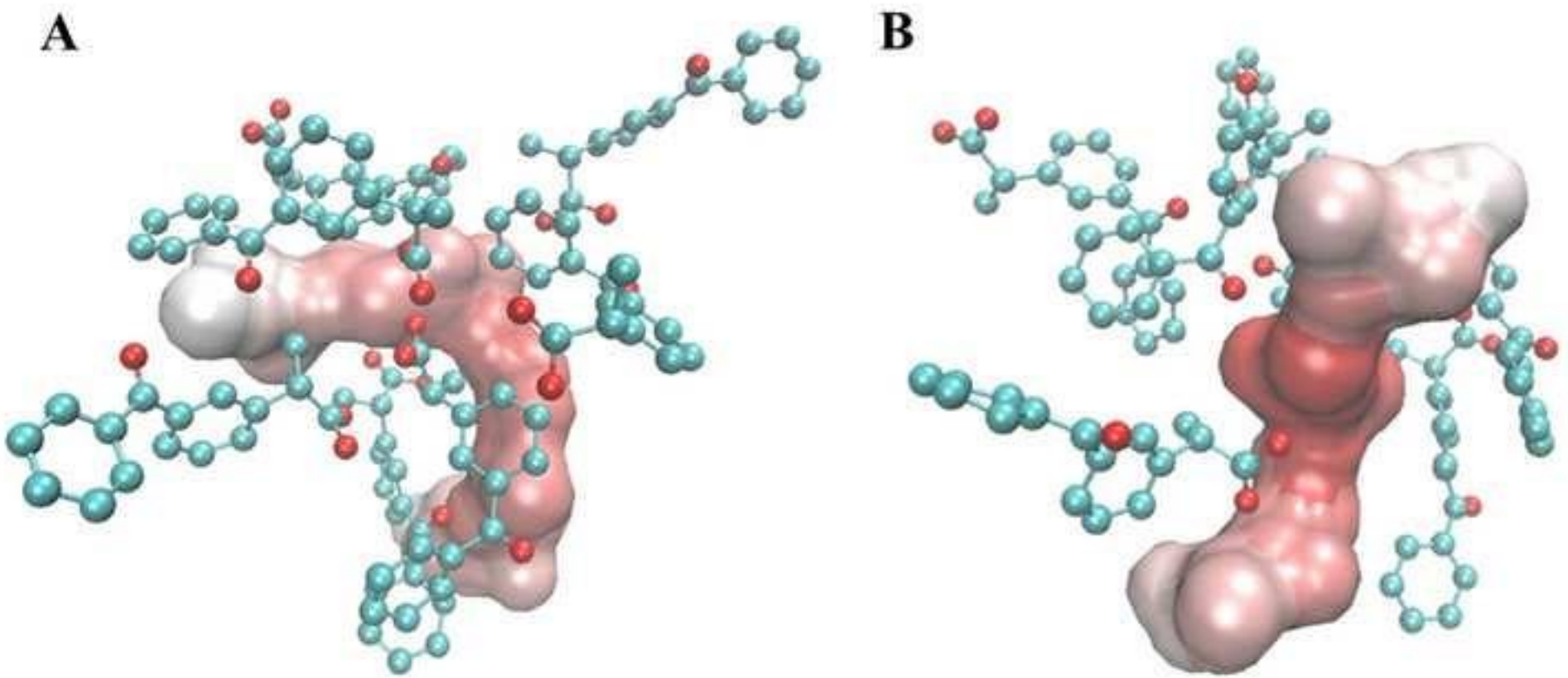
A
B